

Effect of energetic electron irradiation on graphene and graphene field-effect transistors

Isaac Childres^{1,2}, Michael Foxe^{4,#}, Igor Jovanovic^{4,#}, Yong P. Chen^{1,2,3}

¹*Department of Physics, Purdue University, West Lafayette, IN, 47907*

²*Birck Nanotechnology Center, Purdue University, West Lafayette, IN, 47907*

³*School of Electrical and Computer Engineering, Purdue University, West Lafayette, IN, 47907*

⁴*School of Nuclear Engineering, Purdue University, West Lafayette, IN, 47907*

[#]*Current Address: Department of Mechanical and Nuclear Engineering, The Pennsylvania State University, University Park, PA, 16802, USA*

ABSTRACT

We present a study of the effects of electron-beam irradiation on the Raman spectra and electronic transport properties of graphene and the operation of graphene field-effect transistors (GFET). Exposure to a 30 keV electron-beam causes negative shifts in the charge-neutral point (CNP) of the GFET, interpreted as due to n-doping in the graphene from the interaction of the energetic electron beam with the substrate. The electron beam is seen to also decrease the carrier mobilities and minimum conductivity of the graphene, as well as increase the intensity of the Raman D peak, all of which indicate defects generated in the graphene. We also study the relaxation of electronic properties after irradiation. The findings are valuable for understanding the effects of radiation damage on graphene and for the development of radiation-hard graphene-based electronics.

Keywords: Graphene, defects, electron beam, Raman spectroscopy, electronic transport, radiation detection

1. INTRODUCTION

Graphene has been the focus of much research in material science and nanotechnology due to its many unique properties and potential in device applications. Many studies report on graphene's very high electrical conductivity^{1,2} at room temperature, and it is discussed as having potential for use in next-generation transistors³ and novel nano-sensors⁴. It is important to understand the radiation-hardness of graphene in order to operate graphene-based devices in harsh environments such as outer space⁵. In addition, graphene may also have applications as a radiation detector⁶.

Here we present a study of extended exposure of energetic electrons on graphene and the effect of this exposure on its Raman spectra and electronic transport properties. Our interest in the change in graphene, especially its degree of degradation caused by electron bombardment, is threefold: 1) electron beams are a commonly used tool in both imaging of graphene, (e.g. scanning electron microscopy (SEM) and transmission electron microscopy (TEM)), and fabricating graphene devices using electron-beam lithography; 2) such studies are important to develop graphene-based radiation-hard electronics which can stand up to extreme conditions⁵; and 3) our group is currently developing an ionizing radiation detector which uses the field effect in graphene, as in Figure 1(c)⁶. Radiation produces primary Compton electrons in the semiconductor substrate supporting graphene. The electrons travel through the substrate and can reach the graphene surface. Therefore, understanding how energetic electrons interact with the graphene is important for the reliability and long-term robustness of such sensors.

2. METHODS

Our graphene samples are fabricated by micromechanical exfoliation¹ of highly ordered pyrolytic graphite (ZYA grade) onto a boron-doped Si wafer covered with 300 nm of SiO₂. Single-layer graphene flakes, typically around 100 μm² in size, are identified using color contrast with an optical microscope⁷, and then confirmed with Raman spectroscopy (using a 532 nm excitation laser, with a power of 0.2 mW)⁸. Graphene field-effect devices are subsequently fabricated using electron-beam lithography. The electrical contacts (5 nm-thick chromium and 65 nm-thick gold) are fabricated by electron-beam evaporation. Figure 1(b) shows a typical graphene field-effect device once the fabrication is complete.

A graphene device is then placed in a scanning electron microscope (EVO40, Figure 1(a)) under high vacuum (10⁻⁶ torr). An area of 25 μm by 25 μm (shown in Figure 1(b) inset as the white-bordered box indicated by the arrow), including the graphene flake on the device, is continuously scanned by the electron beam. Possible paths of these energetic electrons through the device are modeled in Figure 1(d). The beam's kinetic energy is 30 keV, the same energy that is used for our lithography and imaging processes, and the beam current is 0.133 nA. The accumulated time exposed to the electron-beam (T_e) determines the accumulated irradiation dosage (DOS) (e.g. $T_e = 60$ s gives $DOS = 100$ e⁻/nm²). In comparison, the typical exposure used in our lithography process is around 1 e⁻/nm². SEM imaging typically exposes samples to at least 100 e⁻/nm².

After each successive exposure, the graphene device is removed from the scanning electron microscope, and room-temperature electrical or Raman measurements are promptly performed. Field-effect electrical measurements with the p-doped Si substrate as the back gate are performed using a probe station filled with argon gas at 1 atm. Raman spectra are taken with a 532 nm excitation laser in an ambient atmosphere. To study the long-term evolution of the field-effect, we also exposed 2 additional graphene devices to 100 e⁻/nm² and then monitored their electrical characteristics periodically, one under ambient conditions and the other under rough vacuum (10⁻³ torr).

3. RESULTS AND ANALYSIS

3.1 Raman Spectroscopy

Prior to exposure, the Raman spectrum of device “A” shows the signature for pristine single-layer graphene, with a G peak at ~1580 cm⁻¹ and a 2D peak at ~2690 cm⁻¹, with a ratio of the intensities of the 2D and G peaks, I_{2D}/I_G , of 3.4⁷. We observe a small presence of a disorder-induced D peak at ~1350 cm⁻¹, most likely caused by device fabrication techniques.

Figure 2 shows how the Raman spectra evolve with increased electron-beam irradiation. Representative spectra are shown in Figure 2(a), demonstrating the increase of the D peak, as well as the emergence of peaks at ~1620 cm⁻¹ (D') and ~2940 cm⁻¹ (D+D'). After higher exposures, these extra peaks attenuate.

This can be seen more clearly in Figure 2(b), which shows the progression of the peak intensity ratios (I_D/I_G and I_{2D}/I_G) as functions of DOS . The dependence of the ratio of the intensities of the D and G peaks, I_D/I_G , on DOS shows 2 different behaviors in the regimes of “low” ($DOS < 800$ e⁻/nm²) and “high” ($DOS > 800$ e⁻/nm²) defect densities (referred to as “nanocrystalline graphene” and “mainly sp² amorphous carbon” phases respectively in Ref. 9). I_D/I_G begins at ~0 before the electron-beam exposure and then increases with increasing DOS in the low-defect-density regime to ~3 after 800 e⁻/nm², and I_D/I_G then decreases with further increasing DOS in the high-defect-density regime to ~1 for $DOS = 4000$ e⁻/nm². This non-monotonic behavior of I_D/I_G was also observed in other recent studies of disordered graphene^{10,11}.

We also note a small overall decrease in I_{2D}/I_G in the low defect regime, but then the ratio levels off at ~2.2 after higher exposures.

3.2 Electronic Transport Measurements

We can characterize our graphene's electronic properties by performing 4-terminal conductance measurements under a varying back gate voltage between the doped Si substrate and the graphene. Graphene is a zero-gap

semiconductor, and as the back gate voltage is varied, there is a voltage value where the majority charge carrier density shifts from p-type to n-type. This is the point of minimum conductivity (σ_{min}), because the average charge density is zero at this charge-neutral “Dirac” point (CNP)¹. In addition to tracking the CNP (Figure 3(a)) and σ_{min} (Figure 3(c)) for increasing amounts of accumulated exposure, we can also extract the electron and hole mobilities (μ_e and μ_h , respectively) by examining the slope of the field-effect curve, conductivity (σ) vs back gate voltage (V_g), where V_g is sufficiently far away from the CNP and the curve is in the linear regime, using

$$\mu = \frac{t}{\epsilon} \times \frac{d\sigma}{dV_g} \quad (1)$$

where $t = 300$ nm is the thickness of the SiO₂ and $\epsilon = 3.9 \times \epsilon_0 = 3.45 \times 10^{-11}$ F/m is the permittivity of the SiO₂¹². The progressions of μ_e and μ_h are shown in Figure 3(b).

Before irradiation, we measure device “B” to have a CNP of 11.5 V, as well as $\mu_h = 4000$ cm²/Vs, $\mu_e = 4900$ cm²/Vs and $\sigma_{min} = 277$ μ S. After a 500 e⁻/nm² exposure, all electronic properties of the device decrease significantly, with a CNP of -21.1 V, $\mu_h = 1150$ cm²/Vs, $\mu_e = 1200$ cm²/Vs and $\sigma_{min} = 147$ μ S. Electron-beam irradiation past 500 e⁻/nm² further decreases the mobility and conductivity of the sample and increases the CNP, though the change is not nearly as great as the initial exposure. In fact, both mobilities appear to saturate at ~ 1000 cm²/Vs while σ_{min} saturates at ~ 130 μ S. It is interesting to note that despite this saturation, graphene continues to get more disordered for these high dosages, as made evident by the progression of I_D/I_G .

To confirm that these changes to the field-effect measurements are caused by the electron bombardment and not another aspect of our procedure (e.g. the high vacuum of the SEM), we also prepare a control device “C” and subject it to the same procedure and measurements except the electron beam was not turned on. The simulated exposure has a much smaller effect on the device “C,” seen in Figure 3. The hole mobility slightly increases while the CNP decreases, both of which we believe to be caused by dopant impurities such as water molecules from the air being desorbed under high vacuum.

3.3 Relaxation of electronic transport properties after irradiation

We also investigate the long-term evolution of the electronic properties of our graphene devices after a relatively low dosage of irradiation. Figure 4 shows the progression of the electronic properties over time for 2 irradiated devices “D” and “E.” The field-effect of device “D” is measured periodically for 2 days while it remains in an ambient environment after exposure (Figure 4(a,b)). To investigate what effects vacuum might have on the relaxation, device “E” is placed in a rough vacuum after exposure, where its field-effect is also measured periodically (Figure 4(c,d)). After 2 days, it is removed from vacuum and we continue to monitor it for an additional 2 days.

For device “D,” after seeing the expected drop in all measured quantities after exposure, we immediately see the CNP shift back toward the positive, though it has not reached its original value after 2 days (ending at ~ 15 V compared with 17.3 V before irradiation). The mobilities and conductivity show no such upshift over time. These quantities fluctuate but remain relatively constant after exposure.

For device “E,” after exposure, the CNP decreases from 19.3 V to 3 V, then decreases further in vacuum to -1.2 V. Upon removal from vacuum, the CNP increases to 5.7 V, still significantly lower than its value before irradiation. After exposure, σ_{min} decreases from 305 μ S to 266 μ S, then increases significantly in vacuum to 385 μ S. Upon removal from vacuum, σ_{min} decreases to 324 μ S, a value higher than its original value before irradiation. Electron and hole mobilities both decrease due to initial irradiation, then increase while in vacuum, followed by a decrease of a comparable magnitude when removed from vacuum. The rich behavior we are observing may be a combination of multiple effects in these measurements – both the irradiation charge leaking off the substrate and the desorption/adsorption of dopant molecules from the air. More study is required to fully understand the nature of the relaxation after irradiation.

4. DISCUSSION

We can interpret most of the negative shift of the CNP as due to the interaction of the SiO₂/Si substrate with energetic electron-beam irradiation. This irradiation generates electron-hole pairs, and the less-mobile holes can get trapped at the SiO₂/Si interface to create an effective extra positive bias, attracting electrons in the graphene and resulting in a decreased CNP. This is similar to the negative shift of threshold voltage shift well-known in irradiated metal-oxide-semiconductor field-effect transistors (MOSFETs)⁵. Evidence of this substrate doping was also found in a previous report, where it was also demonstrated that the doping was much less in suspended graphene devices¹³.

The negative shift of the conductivity and mobility, however, is caused by a separate non-reversible mechanism. With the emergence of characteristic disorder peaks in the Raman spectra and the progression of the intensity ratio I_D/I_G through the regimes of low and high defect density indicative of decreasing crystalline domain size⁹, we conclude that electron-beam irradiation is indeed creating defects within the carbon lattice of graphene and these defects increase the scattering rates of charge carriers in the material, lowering conductivity and carrier mobility. Interestingly, however, these effects seem to saturate at higher exposures, indicating that further structural disorder in graphene may not strongly affect its electronic properties.

5. CONCLUSION

In summary, we have studied properties of graphene after it is subject to electron-beam irradiation. We hope our work will add some insight into how graphene-based devices are affected by other types of irradiations. In this study, we show evidence of irradiation-induced disorder using Raman spectra and electronic measurements. There is an emergence of the characteristic Raman D peak. We also observe a significant loss of conductivity and carrier mobility, both of which saturate at high exposure levels. Irradiation also causes a temporary charging of the substrate, as made evident by the negative shift of the CNP. We conclude that care should be taken when using e-beam-based lithography or imaging on graphene, as prolonged exposure could cause a degradation of graphene properties. In addition, this study is valuable for understanding the effects of radiation damage on graphene and for the development of radiation-hard graphene-based electronics.

REFERENCES

- [1] Geim A. K., Novoselov K. S., "The Rise of Graphene," *Nature Mater.* 6, 183 (2007)
- [2] Berger C., Song Z., Li X., Wu X., Brown N., Naud C., Mayou D., Li T., Hass J., Marchenkov A. N., Conrad E. H., First P. N., de Heer W. A., "Electron Confinement and Coherence in Patterned Epitaxial Graphene," *Science* 312, 1191 (2006)
- [3] Schwierz F., "Graphene Transistors," *Nature Nanotech.* 5, 487 (2010)
- [4] Schedin F., Geim A. K., Morozov S. V., Hill E. W., Blake P., Katsnelson M. I., Novoselov K. S., "Detection of Individual Gas Molecules Adsorbed on Graphene," *Nature Mater.* 6, 652 (2007)
- [5] Claeys C., Simoen E., [Radiation Effects in Advanced Semiconductor Materials and Devices] Springer, Berlin, (2002)
- [6] Jalilian R., Foxe M., Lopez G., Childres I., Jovanovic I., Chen Y. P., "Graphene Based Sensors for Detecting Ionizing Radiation," *IEEE NSS Conf. Records N05-1* (2009)
- [7] Blake P., Hill E. W., Castro Neto A. H., Novoselov K. S., Jiang D., Yang R., Booth T. J., Geim A. K., "Making Graphene Visible," *Appl. Phys. Lett.* 91, 063124 (2007)
- [8] Ferrari A. C., Meyer J. C., Scardaci V., Casiraghi C., Lazzeri M., Mauri F., Piscanec S., Jiang D., Novoselov K. S., Roth S., Geim A. K., "Raman Spectrum of Graphene and Graphene Layers," *Phys. Rev. Lett.* 97, 187401 (2006)
- [9] Ferrari A. C., "Raman Spectroscopy of Graphene and Graphite," *Solid State Commun.* 143, 47 (2007)
- [10] Teweldebrhan D., Balandin A. A., "Modification of Graphene Properties Due to Electron-Beam Irradiation," *Appl. Phys. Lett.* 94, 013101 (2009)

- [11] Childres I., Jauregui L. A., Tian J., Chen Y. P., "Effect of Oxygen Plasma Etching on Graphene Studied Using Raman Spectroscopy and Electronic Transport Measurements," *New J. Phys.* 13, 025008 (2011)
- [12] Novoselov K. S., Geim A. K., Morozov S. V., Jiang D., Zhang Y., Dubonos S. V., Grigorieva I. V., Firsov A. A., "Electric Field Effect in Atomically Thin Carbon Films," *Science* 306, 666 (2004)
- [13] Childres I., Jauregui L. A., Foxe M., Tian J., Jalilian R., Jovanovic I., Chen Y. P., "Effect of Electron-Beam Irradiation on Graphene Field Effect Devices," *Appl. Phys. Lett.* 97, 173109 (2010)

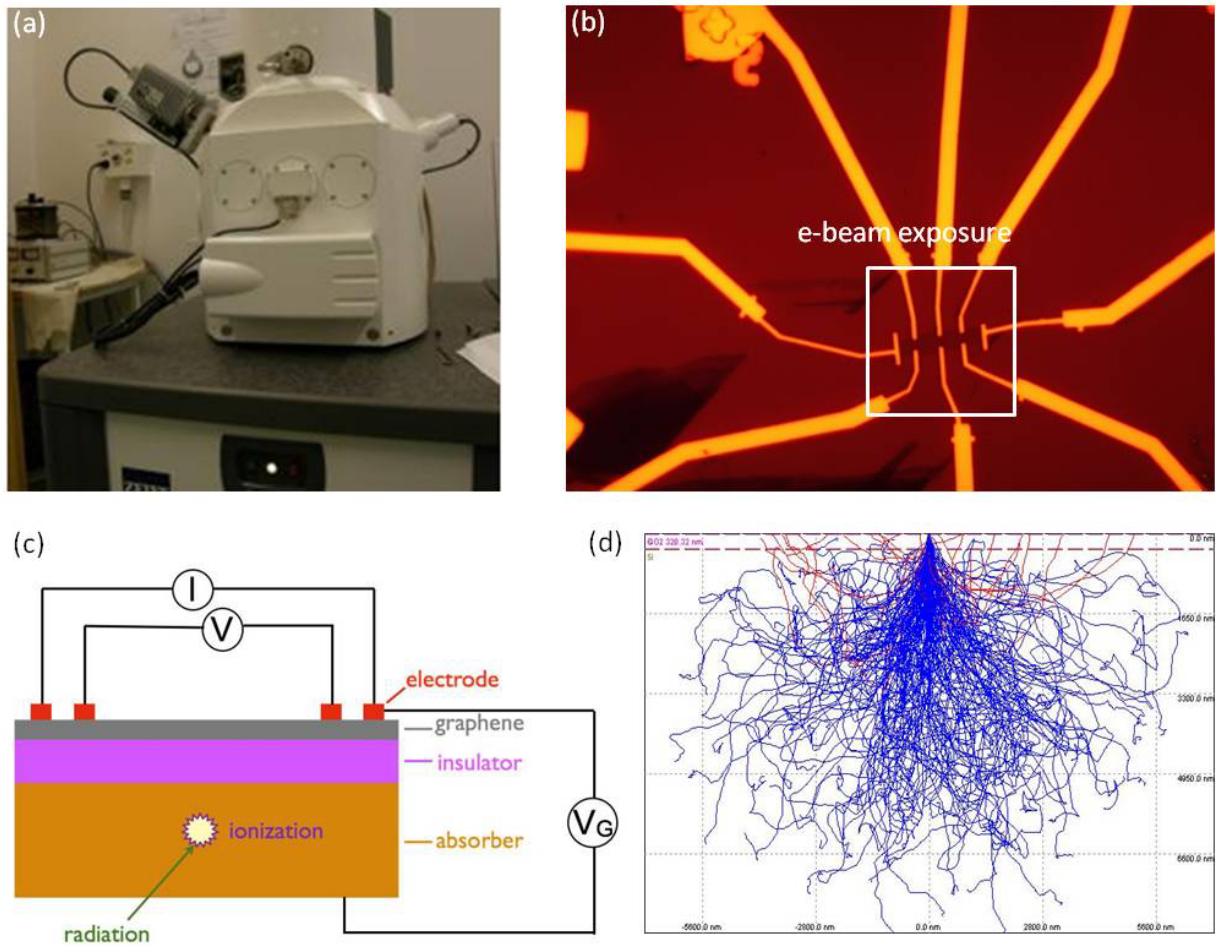


Figure 1. (a) A scanning electron microscope used to expose graphene devices to electron-beam irradiation. (b) An optical image of a typical graphene device with the $25\ \mu\text{m}$ by $25\ \mu\text{m}$ area exposed to electron-beam irradiation indicated by the white box. (c) Schematic of a graphene field-effect transistor (GFET). Results in this paper are obtained using GFETs with heavily doped Si substrates. Using undoped substrates, GFETs can be used as radiation detectors. (d) Monte Carlo (using CASINO) simulation of possible paths of secondary electrons ionized by a 30 keV electron through a 0.5 mm-thick silicon substrate (the top SiO_2 layer is indicated by the dashed line). In radiation detection, higher energy electrons generated from gamma rays could also pass through the substrate and interact with the graphene.

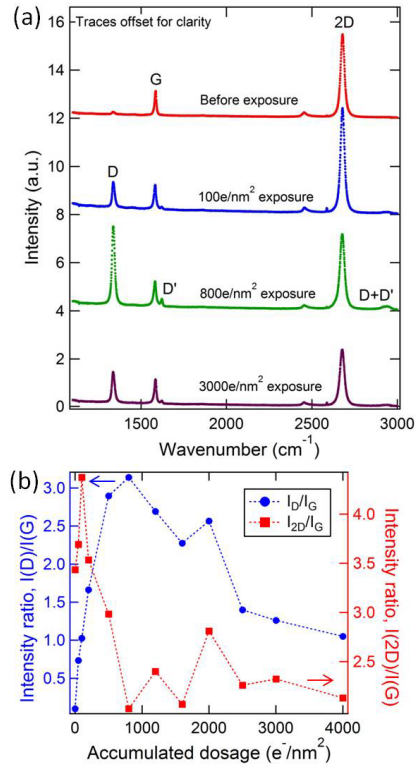


Figure 2. (a) Raman spectra (excitation wavelength 532 nm) for a progression of accumulated electron-beam exposures on graphene device “A.” (b) The full progression of the ratios of Raman peak intensities I_D/I_G and I_{2D}/I_G plotted against the accumulated dosage of energetic electrons.

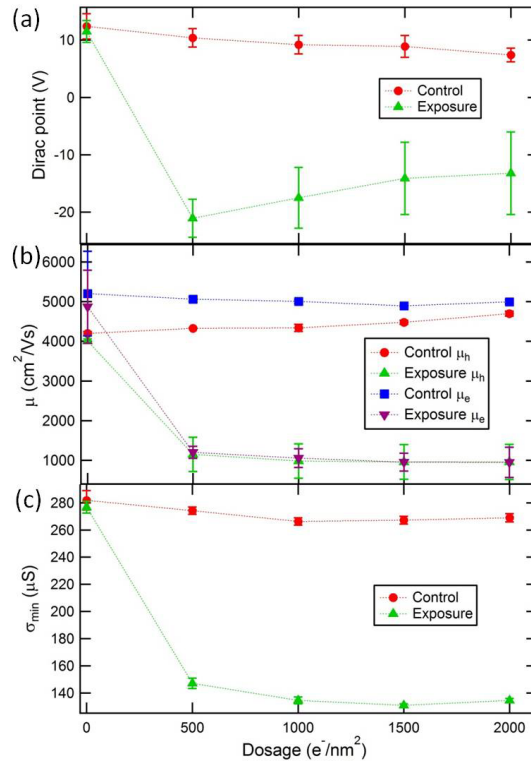


Figure 3. Charge-neutral “Dirac” point (a), electron and hole field-effect mobilities (b) and minimum conductivity (c) of irradiated device “B” and control device “C” as functions of accumulated electron-beam irradiation dosage. The control sample underwent the same procedure as the irradiated sample except that the electron-beam was not turned on for its “irradiation.” Each data point is the average of two measurements from forward and backward gate voltage sweeps. The error bars reflect the variation between the two sweeps.

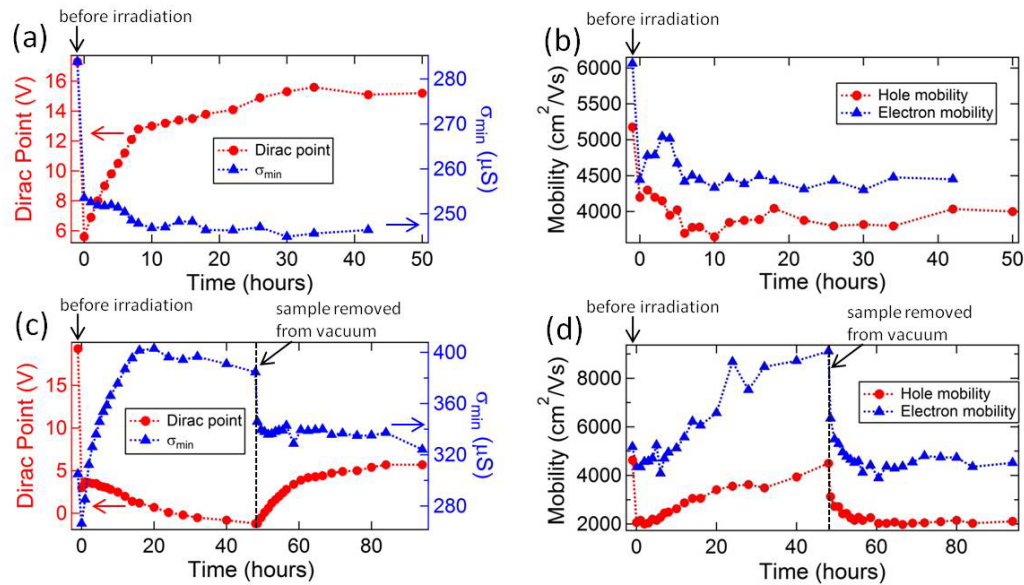


Figure 4. Electrical characteristics measured over time for a device irradiated by $100 e^-/\text{nm}^2$. Dirac point, minimum conductivity (a) and electron and hole field-effect mobilities (b) for device “D” left in an ambient

environment after exposure. Dirac point, minimum conductivity (c) and electron and hole field-effect mobilities (d) for device "E" placed immediately in vacuum after irradiation, then removed after 2 days. The first point in each plot is the value before irradiation.